Published in final edited form as:
Chemistry. 2013 October 11; 19(42): 14112–14118. doi:10.1002/chem.201300107.

Synthesis, Characterization, and Reactivity of Cobalt(III)–Oxygen Complexes Bearing a Macrocyclic N-Tetramethylated Cyclam Ligand

Doyeon Kim[a], **Jaeheung Cho**[a,b], **Yong-Min Lee**[a], **Ritimukta Sarangi**[c], and **Wonwoo Nam**[a]
Wonwoo Nam: wwnam@ewha.ac.kr
[a]Department of Bioinspired Science, Department of Chemistry and Nano Science, Ewha Womans University, Seoul 120-750 (South Korea)
[b]Department of Emerging Materials Science, DGIST, Daegu 711-873 (South Korea)
[c]Stanford Synchrotron Radiation Lightsource, SLAC National Accelerator Laboratory, Menlo Park, California 94025 (USA)

Abstract

Mononuclear metal–dioxygen species are key intermediates that are frequently observed in the catalytic cycles of dioxygen activation by metal-loenzymes and their biomimetic compounds. In this work, a side-on cobalt-(III)–peroxo complex bearing a macro-cyclic N-tetramethylated cyclam (TMC) ligand, $[Co^{III}(15\text{-}TMC)(O_2)]^+$, was synthesized and characterized with various spectroscopic methods. Upon protonation, this cobalt(III)–peroxo complex was cleanly converted into an end-on cobalt(III)–hydroperoxo complex, $[Co^{III}(15\text{-}TMC)(OOH)]^{2+}$. The cobalt(III)–hydroperoxo complex was further converted to $[Co^{III}(15\text{-}TMC\text{-}CH_2\text{-}O)]^{2+}$ by hydroxylation of a methyl group of the 15-TMC ligand. Kinetic studies and ^{18}O-labeling experiments proposed that the aliphatic hydroxylation occurred via a Co^{IV}–oxo (or Co^{III}–oxyl) species, which was formed by O–O bond homolysis of the cobalt(III)–hydroperoxo complex. In conclusion, we have shown the synthesis, structural and spectroscopic characterization, and reactivities of mono-nuclear cobalt complexes with peroxo, hydroperoxo, and oxo ligands.

Keywords

aliphatic hydroxylation; bioinorganic chemistry; cobalt; macrocyclic ligands; oxygen

Introduction

Oxygen-coordinating metal species, such as metal–peroxo,–hydroperoxo, and –oxo complexes (Scheme 1), have been frequently invoked as reactive intermediates in the catalytic cycles of dioxygen activation by metalloenzymes, such as heme and nonheme iron monooxygenases and copper-containing enzymes.[1] In biomimetic studies, synthetic analogues of these active oxygen intermediates have been intensively investigated to understand their structures, mechanisms of interconversion, and the factors that control their chemical reactivities in oxidation reactions.[2] In those studies, it has been shown that supporting ligands play an important role in tuning the geometric and electronic structures,

Correspondence to: Wonwoo Nam, wwnam@ewha.ac.kr.
Supporting information for this article is available on the WWW under http://dx.doi.org/10.1002/chem.201300107.

stabilities, and reactivities of the oxygen-coordinating metal complexes. One notable example of the supporting ligands is *N*-tetramethylated cyclam (TMC) and its derivatives,[3] which have proved to be versatile ligands in the biomimetic chemistry of dioxygen activation by metal complexes (see Scheme 2 for the ligand structures of *n*-TMC).[4] A variety of metal–TMC complexes with oxo, superoxo, peroxo, and hydroperoxo ligands have been synthesized and spectroscopically and/or structurally characterized.[2h, 5–10] In particular, the first high-resolution crystal structures of mononuclear nonheme iron(IV)–oxo and iron(III)–peroxo complexes, such as $[Fe^{IV}(14\text{-TMC})(O)]^{2+}$ and $[Fe^{III}(14\text{-TMC})(O_2)]^{+}$, were successfully obtained by using the 14-TMC macrocyclic ligand.[7a, 10a] It was also shown that the iron(III)–peroxo complex $[Fe^{III}(14\text{-TMC})(O_2)]^{+}$ was cleanly converted to the corresponding iron(III)–hydroperoxo complex, $[Fe^{III}(14\text{-TMC})(OOH)]^{2+}$, upon protonation; this was followed by clean conversion of the iron(III)–hydroperoxo complex to an iron(IV)–oxo complex, $[Fe^{IV}(14\text{-TMC})(O)]^{2+}$, through homolytic O–O bond cleavage.[7a] As part of our ongoing efforts to elucidate the chemistry of metal–O_2 complexes, we synthesized a novel cobalt(II) complex bearing a 15-TMC ligand, $[Co^{II}(15\text{-TMC})]^{2+}$ (**1**; see the structure of the 15-TMC ligand in Scheme 2) and used it for the synthesis of cobalt(III)–peroxo and –hydroperoxo complexes ($[Co^{III}(15\text{-TMC})(O_2)]^{+}$ (**2**) and $[Co^{III}(15\text{-TMC})(OOH)]^{2+}$ (**3**)).[11] We also show that the cobalt(III)–hydroperoxo complex (**3**) is cleanly converted to $[Co^{III}(15\text{-TMC-}CH_2\text{-}O)]^{2+}$ (**4**) by hydroxylation of an *N*-CH_3 group of the 15-TMC ligand. In the latter reaction, we propose that the hydroperoxide group in **3** is homolytically cleaved to generate a high-valent cobalt(IV)–oxo (or cobalt(III)–oxyl) intermediate as an active oxidant that effects the C–H bond activation of the 15-TMC ligand.

Results and Discussion

The starting cobalt complex, $[Co^{II}(15\text{-TMC})(CH_3CN)_2]^{2+}$ ([**1**•$(CH_3CN)_2$]), was synthesized by the reaction of equimolar amounts of $Co(ClO_4)_2$•$6H_2O$ and 15-TMC in CH_3CN (Figure 1 a for X-ray crystal structure; Tables S1 and S2 and Figures S1 and S2 in the Supporting Information for structural and spectral data, respectively). Addition of aqueous H_2O_2 (10 equiv relative to **1**) to a reaction solution containing **1** and triethylamine (TEA; 5 equiv relative to **1**) in CH_3CN at 0 °C afforded the green intermediate **2** with absorption bands at 464 ($\varepsilon = 120_M{}^{-1}cm^{-1}$) and 615 nm ($\varepsilon = 90_M{}^{-1}cm^{-1}$; Figure 2 a). Complex **2** was metastable at 0 °C ($t_{1/2} \approx 2$ h), which allowed us to characterize it with various spectroscopic techniques. The ESI mass spectrum of **2** exhibits a prominent signal at *m*/*z* 361.1 (Figure 2 b), and the mass and isotope distribution pattern correspond to $[Co(15\text{-TMC})(O_2)]^{+}$ (calcd: *m*/*z* 361.2). When the reaction was carried out with isotopically labeled $H_2{}^{18}O_2$, a mass peak corresponding to $[Co(15\text{-TMC})(^{18}O_2)]^{+}$ appeared at *m*/*z* 365.1 (calcd: *m*/*z* 365.2; Figure 2b, inset). The observation of a four-mass-unit upshift upon substitution of ^{16}O atoms with ^{18}O atoms indicates that **2** contains an O_2 unit. The X-band EPR spectrum of **2** is silent at 4.3 K, and the determination of the spin state of **2** by using the ^1H NMR method of Evans[12] clearly indicates that **2** is a low-spin state ($S = 0$) cobalt(III) d^6 species.[8] The oxidation of **1** (Co^{2+}) to **2** (Co^{3+}) was confirmed by using Co K-edge XAS data, which show a clear shift in the pre-edge and rising edge to higher energy upon going from **1** to **2** (Figure 3 a; Table S3 in the Supporting Information). Figure 3b shows the Fourier transform and corresponding non-phase-shift-corrected EXAFS data for **2**. The EXAFS data are consistent with a six-coordinate site in **2** with two short Co–O bond lengths of 1.89 Å and four Co–N bond lengths of 2.07 Å. Based on the spectroscopic and structural characterization, complex **2** is assigned as a cobalt(III) complex with a ‘side-on’ peroxo group, $[Co^{III}(15\text{-TMC})(O_2)]^{+}$.

Addition of $HClO_4$ (10 equiv) to a solution of **2** in CH_3CN at 0 °C immediately generated the violet intermediate **3** with electronic absorption bands at 566 and 805 nm; this was followed by the conversion ($t1/2 \approx 90$ s) of **3** to a new purple species, **4**, with electronic

absorption bands at 531 and 740 nm (Figure 2 a). In the conversion of **3** to **4**, the rate, k_{obs}, was determined to be 3.7(3) × 10^{-3} s^{-1} at 0 °C (Figure S3 in the Supporting Information), and isosbestic points were observed at 555, 640, and 820 nm (Figure 2 a, inset). In addition, the temperature dependence of the k_{obs} value was determined in the range of 253–283 °C, and the results gave rise to an Eyring plot that afforded activation parameters of $\Delta H^{\ddagger}$ = 104(6) $kJ^{-1}mol^{-1}$ and $\Delta S^{\ddagger}$= 90(5) $Jmol^{-1}K^{-1}$ (Figure S4 in the Supporting Information). Complex **3** was EPR silent, and the spin state of the cobalt ion was determined to be $S = 0$ by using the Evans ^{1}H NMR method.[12] In addition, the similarity in the Co K-edge XAS rising-edge energy positions (Figure 3 a; Table S4 in the Supporting Information) indicates that the oxidation state of **3** is the same as that of **2** (namely, Co^{3+}). FEFF program fits to the EXAFS data are consistent with one short Co–O bond length of 1.86 Å, four Co–N bond lengths of 2.04 Å, and one Co–N bond length of 2.19 Å, which supports a cobalt(III) complex with an 'end-on' hydroperoxo binding and a *trans*-axial acetonitrile ligation, $[Co^{III}(15\text{-}TMC)(O_2H)(CH_3CN)]^{2+}$.

Intermediate **3** rapidly reverted back to **2** upon addition of tetramethylammonium hydroxide (TMAH; 3 equiv), and addition of $HClO_4$ to the resulting solution of **2** regenerated **3** quantitatively. This reversible cycle could be repeated several times, which suggests that **2** and **3** are interconverted through the acid–base chemistry proposed in Scheme 3; such an interconversion has been well demonstrated in non-heme iron(III)–peroxo and iron(III)–hydroperoxo species.[13] Thus, the above evidence for this acid–base interconversion further supports the identification of intermediates **2** and **3** as the cobalt(III)–peroxo, $[Co^{III}(15\text{-}TMC)(O_2)]^{+}$, and cobalt-(III)–hydroperoxo species, $[Co^{III}(15\text{-}TMC)(O_2H)]^{2+}$, respectively.

As mentioned above, the cobalt(III)–hydroperoxo species, **3**, cleanly converts to the thermally stable product **4**. We thus characterized **4** with various spectroscopic methods and X-ray crystallography. The ESI mass spectrum of **4** exhibits a signal at *m*/*z* 192.5 (Figure 4), and the mass and isotope distribution pattern correspond to $[Co^{III}(15\text{-}TMC\text{-}CH_2\text{-}O)\text{-}(CH_3CN)]^{2+}$ (calcd: *m*/*z* 192.6). When the reaction was carried out with **3** prepared with isotopically labeled H_2 $^{18}O_2$, the mass peak corresponding to **4** shifted to *m*/*z* 193.5 (calcd: *m*/*z* 193.6; Figure 4), which indicates that **4** contains an oxygen atom. Furthermore, when the reaction was carried out with deuterated $[Co^{II}(15\text{-}TMC\text{-}(CD_3)_4)]^{2+}$ (**1**-CD_3), a mass peak corresponding to $[Co^{III}(15\text{-}TMC\text{-}(CD_3)_3\text{-}CD_2\text{-}O)(CH_3CN)]^{2+}$ (**4**-CD_3) appeared at *m*/*z* 198.0 (calcd: *m*/*z* 198.1; Figure 4; see below). Complex **4** was EPR silent at 4.3 K, and the spin state of the cobalt ion was determined to be $S = 0$ by the Evans ^{1}H NMR method.[12]

Complex **4** was further characterized by X-ray diffraction analysis (Tables S1 and S2 in the Supporting Information). As shown in the molecular structure in Figure 1b, complex **4** has a six-coordinate cobalt ion with four nitrogen atoms from the macrocyclic 15-TMC ligand in equatorial positions, one axial hydroxide ligand, and a *trans*-axial oxygen atom from an alkoxide group. Thus, the crystal structure clearly illustrates the hydroxylation of a ligand methyl group and the ligation of the resulting O atom of the alkoxide to the cobalt ion.

We then investigated the mechanism of the conversion of **3** to **4** (i.e., the hydroxylation of the *N*-methyl group by a cobalt(III)–hydroperoxo species). Three possible mechanisms were considered (Scheme 4): One is the direct C–H bond activation of the methyl group by the hydroperoxo ligand in **3**, which would generate H_2O, Co^{III}–O•, and N– CH_2• (pathway A).[14] Radical coupling between Co^{III}–O• and N–CH_2• would produce the oxygenated product **4**. In this direct C–H bond activation by the hydroperoxo group, a high kinetic isotope effect (KIE) value (>1) would be expected with the deuterated *N*-methyl group. Since the KIE value of 1 was obtained in the conversion of **3** to **4** (k_{obs} = 3.7(3) × 10^{-3} $s^{-}1$ for **3**-(CH_3) and 3.4(4) × 10^{-3} s^{-1} for **3**-(CD_3)), we ruled out the mechanism of direct C–H bond activation by the hydroperoxo ligand in **3**.[15] The other possibilities are O–O bond

cleavage of **3** by heterolysis or homolysis. Heterolytic cleavage of the O–O bond would generate Co^{IV}–O• and OH^- (pathway B). H-atom abstraction by Co^{IV}–O• and a rebound process would produce **4**. Addition of a proton would facilitate the heterolytic cleavage of the O–O bond, in which one of the oxygen atoms forms an oxyl radical and the other is released as water.[1b, 16] However, we found no proton-concentration effect on the rate of the O–O bond cleavage of **3** (Table S5 in the Supporting Information). Thus, homolytic cleavage is the most likely mechanism (pathway C), because it is consistent with KIE = 1 and a lack of proton-concentration effect in the kinetic experiments. The homolytic cleavage of the hydroperoxo O–O bond would produce CoIII–O• and • OH species, which is proposed to be a rate-determining step. The • OH species abstracts an H atom from the methyl group to afford H_2O; this is followed by radical coupling between CoIII–O• and N–CH_2• to yield **4**. As a precedent, we have recently shown an example of O–O bond homolysis of an iron(III)–hydroperoxo complex that leads to the generation of an iron(IV)–oxo complex.[7a]

The reactivity of **3** toward external substrates was investigated as well. Upon addition of substrates, such as xanthene, anthracene, cyclohexadiene, and cyclohexane, to the solution of **3**, we could not observe any difference in the k_{obs} value. Furthermore, product analysis of the reaction solutions revealed that no oxidized products were formed in these reactions. The results demonstrate that **3** is not capable of reacting with external substrates because the intramolecular hydroxylation occurs at a fast rate under the reaction conditions.

Conclusion

We have shown the synthesis of a cobalt(III)–peroxo (**2**) complex with a macrocyclic 15-TMC ligand and its conversion to a cobalt(III)–hydroperoxo (**3**) complex upon protonation. The latter species was further converted to give an oxygenated product, **4**, in which an *N*methyl C–H bond of the 15-TMC ligand bound to the Co center was hydroxylated. Kinetic studies support a homolytic O–O bond cleavage of the hydroperoxo ligand in **3** through the formation of a cobalt(III)–oxyl species, which is responsible for the hydroxylation of the *N*-methyl group of the 15-TMC ligand. This study is another step towards understanding formation processes through structural and spectroscopic studies and ligand oxidation reactions, which provide important fundamental information about the aliphatic hydroxylation by metal–O_2(H) and metal–O intermediates.

Experimental Section

Materials

All chemicals obtained from Aldrich Chemical Co. were the best available purity and were used without further purification unless otherwise indicated. Solvents were dried according to published procedures and distilled under Ar prior to use.[17] H_2 $^{18}O_2$ (90% ^{18}O-enriched, 2% H_2 $^{18}O_2$ in water) and H_2 ^{18}O (95% ^{18}O-enriched) were purchased from ICON Services Inc. (Summit, NJ, USA). Iodosylbenzene (PhIO) and 15-TMC (1,4,8,12-tetramethyl-1,4,8,12-tetraazacyclopentadecane) were prepared according to the literature methods.[18, 19] The [D_{12}]-15-TMC ligand was prepared by mixing an excess amount of [D_2]formaldehyde (20 mmol, 2800 μL) and [D_2]formic acid (20 mmol, 770 μL) with 1,4,8,12-tetraazacyclopentadecane (1.5 mmol, 33 mg). The mixture was heated to reflux for 12 h. After cooling, an aqueous solution of NaOH was added to the mixture. The resulting solution was extracted with $CHCl_3$ (3 × 20 μL). The combined extracts were dried over Na_2SO_4 and $CHCl_3$ was removed by evaporation under reduced pressure: ESI-MS (CH_3CN): *m/z* 283.3 [[D_{12}]-15-TMC+H]$^+$; ^{1}H NMR (CD_3CN, 400 MHz): δ = 2.46 (s, 4 H), 2.39 (t, 12H), 1.60 ppm (q, 6 H).

Instrumentation

UV/Vis spectra were recorded on a Hewlett Packard 8453 diode array spectrophotometer equipped with a UNISOKU scientific instrument for low-temperature experiments. Electrospray-ionization mass spectra were collected on a Thermo Finnigan LCQ Advantage MAX quadrupole-ion-trap instrument (San Jose, CA, USA), by infusing samples directly into the source with a manual method. The spray voltage was set at 4.2 kV and the capillary temperature at 80°C. ^{1}H NMR spectra were measured with Bruker DPX-400 spectrometer. The effective magnetic moments were determined by using the modified ^{1}H NMR method of Evans at −20 °C.[12] A WILMAD coaxial insert (sealed capillary) tube containing the blank [D_3]acetonitrile solvent (with 1.0% tetramethylsilane (TMS)) only was inserted into the normal NMR tubes containing the complexes (8.0 mM) dissolved in [D_3]acetonitrile (with 0.05% TMS). The chemical shift of the TMS peak (and/or solvent peak) in the presence of the paramagnetic metal complexes was compared to that of the TMS peak (and/or solvent peak) in the inner coaxial insert tube. The effective magnetic moment (μ) was calculated by using the equation $\mu = 0.0618(\Delta\upsilon T/2fM)^{1/2}$, in which f is the oscillator frequency (MHz) of the superconducting spectrometer, T is the absolute temperature, M is the molar concentration of the metal ion, and $\Delta\upsilon$ is the difference in frequency (Hz) between the two reference signals.[12c] CW-EPR spectra were taken at 4.3 K by using an X-band Bruker EMX-plus spectrometer equipped with a dual mode-cavity (ER4116DM). Low temperatures were achieved and controlled by using an Oxford Instruments ESR900 liquid He quartz cryostat with an Oxford Instruments ITC503 temperature and gas-flow controller.

Generation and characterization of [Co^{II}(15-TMC)(CH_3CN)$_2$](ClO_4)$_2$ ([1•(CH_3CN)$_2$](ClO_4)$_2$)

15-TMC (0.33 g, 1.5 mmol) was added to a CH_3CN (50 mL) solution of $Co(ClO_4)_2$•$6H_2O$ (0.71 g, 2.6 mmol). The mixture was heated to reflux for 12 h. After the reaction mixture had cooled, the solvent was removed under vacuum to give a red solid, which was collected by filtration and then washed with methanol several times to remove remaining $Co(ClO_4)_2$•$6H_2O$: Yield: 1.11 g (70%); ESI-MS (CH_3CN; Figure S1 in the Supporting Information): *m/z* 164.8 [Co(15-TMC)]$^{2+}$, 184.9 [Co(15-TMC)(CH_3CN)]$^{2+}$, 205.0 [Co(15-TMC)-(CH_3CN)$_2$]$^{2+}$, 428.1 [Co(15-TMC)(ClO_4)]$^+$; μ_{eff} = 4.3 μ_B; elemental analysis: calcd for $C_{19}H_{40}N_6O_8Cl_2Co$: C 37.39, H 6.61, N 13.77; found: C 37.12, H 6.73, N 13.48; X-ray crystallographically suitable crystals were obtained by slow diffusion of Et_2O into concentrated solutions of **1**.

Generation and characterization of [Co^{III}(15-TMC)(O_2)]$^+$ (2)

Treatment of **1** (4 mM) with H_2O_2 (10 equiv) in the presence of TEA (5 equiv) in CH_3CN (2 mL) afforded the formation of a green solution. [Co(15-TMC)($^{18}O_2$)]$^+$ was prepared by adding H_2 $^{18}O_2$ (10 equiv; 32 μL; 90% ^{18}O-enriched 2% H_2 $^{18}O_2$ in water) to a solution containing **1** (4 mM) and TEA (5 equiv) in CH_3CN (2 mL) at 0°C: UV/Vis (CH_3CN at 0°C; Figure 2a): λ = 464 (ε = 120), 615 nm (90 $M^{-1}cm^{-1}$); ESI-MS (CH_3CN; see Figure 2b): *m/z* 361.1 [Co(15-TMC)(O_2)]$^+$.

Generation and characterization of [Co^{III}(15-TMC)(OOH)]$^{2+}$ (3)

Treatment of **2** (4 mM) with $HClO_4$ (10 equiv) in CH_3CN (2 mL) at 0°C afforded the formation of a purple solution. Titration experiments showed that ten equivalents of $HClO_4$ were required for the full formation of **3** (data not shown): UV/Vis (CH_3CN at 0°C; Figure 2a): λ = 566 (ε = 100), 805 nm (30 $M^{-1}cm^{-1}$).

Generation and characterization of [Co^{III}(15-TMC-CH_2-O)(OH)](ClO_4)-(CH_3CN) ([4• (OH)](ClO_4)(CH_3CN))

A solution of **3** in CH_3CN was allowed to stand for several hours at ambient temperature to change the solution color from purple to violet. Slow diffusion of Et_2O into the resulting solution afforded violet crystals: Yield: 0.26 g (45%); UV/Vis (CH_3CN at 0°C; Figure 2a): λ = 531 (ε = 120), 749 nm (70 $_M{}^{-1}cm^{-1}$); ESI-MS (CH_3CN; Figure 4): *m/z* 192.5 [Co(15-TMC-CH_2-O)(CH_3CN)]$^{2+}$; elemental analysis: calcd for $C_{17}H_{37}N_5O_6ClCo$: C 40.68, H 7.43, N 13.95; found: C 40.29, H 7.28, N 13.73; crystals suitable for X-ray crystallo-graphic analysis were obtained by CH_3CN/Et_2O layering of **4**.

Kinetic measurements

All reactions were run in an 1 cm UV cuvette by monitoring UV/Vis spectral changes of reaction solutions, and rate constants were determined by fitting the changes in absorbances at 550 nm for **2**, 566 nm for **3**, and 531 nm for **4**. Reactions were run at least in triplicate, and the data reported represent the average of these reactions. After the completion of the reactions, pseudo-first-order fitting of the kinetic data allowed the k_{obs} values to be determined.

X-ray crystallography

Single crystals of [Co(15-TMC)(CH_3CN)$_2$](ClO_4)$_2$ and [Co(15-TMC-CH_2-O)(OH)](ClO_4)(CH_3CN) were picked from solutions by a nylon loop (Hampton Research Co.) on a handmade copper plate mounted inside a liquid N_2 Dewar vessel at approximately −40°C and mounted on a goniometer head in an N_2 cryostream. Data collections were carried out on a Bruker SMART APEX II CCD diffractometer equipped with a monochromator in the $Mo_{K\alpha}$ (λ= 0.71073 Å) incident beam. The CCD data were integrated and scaled by using the Bruker SAINT software package, and the structure was solved and refined by using SHELXTL Version 6.12 software.[20] Hydrogen atoms were located in the calculated positions for [Co(15-TMC-CH_2-O)(OH)](ClO_4)-(CH_3CN). Due to the high degree of disorder, however, hydrogen atoms could not be placed in ideal positions for [Co(15-TMC)(CH_3CN)$_2$]-(ClO_4)$_2$. Crystal data for [Co(15-TMC)(CH_3CN)$_2$](ClO_4)$_2$: $C_{19}H_0Cl_2CoN_6O_8$; monoclinic; $P2_1/n$; Z= 2; a= 8.6493(8), b= 15.6174(13), c= 10.7612(9) Å; b= 111.2190(10)°; V= 1355.1(2) Å^3 ; μ = 0.880 mm^{-1}; ρ_{calcd} = 1.397 gcm^{-3} ; R_1 = 0.0865, wR_2 = 0.2603 for 2636 unique reflections; 179 variables. Crystal data for [Co(15-TMC-CH_2-O)(OH)](ClO_4)-(CH_3CN): $C_{17}H_{37}ClCoN_5O_6$; monoclinic; $P2_1/c$; Z= 4; a= 9.6291(3), b= 19.6761(6), c= 12.0095(4) Å; b= 98.974(2)8; V= 2247.51(12) Å^3 ; m= 0.925 mm^{-1}; ρ_{calcd} = 1.483 g cm^{-3} ; R_1 = 0.0699, wR_2 = 0.2470 for 4263 unique reflections, 276 variables. The crystallographic data for [Co-(15-TMC)(CH_3CN)$_2$](ClO_4)$_2$ and [Co(15-TMC-CH_2-O)(OH)](ClO_4)-(CH_3CN) and selected bond distances and angles are listed in Tables S1 and S2, respectively, in the Supporting Information. CCDC 882840 ([Co-(15-TMC)(CH_3CN)$_2$](ClO_4)$_2$) and 882839 ([Co(15-TMC-CH_2-O)(OH)]-(ClO_4)(CH_3CN)) contain the supplementary crystallographic data for this paper. These data can be obtained free of charge from the Cambridge Crystallographic Data Centre via www.ccdc.cam.ac.uk/data_request/cif.

X-ray absorption spectroscopy

The Co K-edge X-ray absorption spectra of **1**–**3** were measured at the Stanford Synchrotron Radiation Laboratory (SSRL) on the unfocussed 20-pole 2T wiggler side-station beam line 7–3 under standard ring conditions of 3 GeV and approximately 100 mA. A Si(220) double crystal monochromator was used for energy selection. A Rh-coated harmonic rejection mirror was used on beam line 7–3 to reject components of higher harmonics. The solid sample for **1** was finely ground with BN into a homogeneous mixture and pressed into a 1

mm aluminum spacer between X-ray transparent 37 μm Kapton tape. The solution samples for **2** and **3** (≈120 μL) were transferred into 2 mm delrin XAS cells with 37 μm Kapton tape windows under synthesis conditions. Both solid and solution samples were immediately frozen after preparation and stored under liquid N_2. During data collection, the samples were maintained at a constant temperature of 15 K by using an Oxford Instruments CF 1208 liquid helium cryostat. Data were measured to k= 15 $Å^{-1}$ on **1** (transmission mode) by using an ionization chamber detector and to k= 15 $Å^{-1}$ on **2** and **3** (fluorescence mode) by using a Canberra Ge 30-element array detector. Internal energy calibration was accomplished by simultaneous measurement of the absorption of a Co foil placed between two ionization chambers situated after the sample. The first inflection point of the foil spectrum was fixed at 7709.5 eV. Data presented here are 2-scan (**1**), 15-scan (**2**), and 15-scan (**3**) average spectra, which were processed by fitting a second-order polynomial to the pre-edge region and subtracting this from the entire spectrum as background. A four-region spline of orders 2, 3, 3, and 3 was used to model the smoothly decaying post-edge region. The data were normalized by subtracting the cubic spline and assigning the edge jump to 1.0 at 7725 eV by using the Pyspline program.[21] Theoretical EXAFS signals λ(k) were calculated by using the FEFF program (Macintosh Version 8.4),[22–24] the crystal structure of **1**, and structural models of **2** and **3** built in Avogadro.[25] The theoretical models were fitted to the data by using the EXAFSPAK program.[26] The structural parameters varied during the fitting process were the bond distance (R), the bond variance (σ_2), which is related to the Debye–Waller factor resulting from thermal motion, and the static disorder of the absorbing and scattering atoms. The nonstructural parameter E_0 (the energy at which k= 0) was also allowed to vary but was restricted to a common value for every component in a given fit. Coordination numbers were systematically varied in the course of the fit but were fixed within a given fit. A comparison of the k^3-weighted Co K-edge EXAFS data for **2** and **3**, along with their non-phase-shift-corrected Fourier transforms (k= 2–14 $Å^{-1}$) is shown in Figure 3. The FEFF program fits to the data are presented in Figure 3 and Table S3 in the Supporting Information. On going from **2** to **3**, the first-shell Fourier transform peak intensity decreases, which indicates a decrease in the coordination number in **3**. The second-shell and third-shell features were fitted with single- and multiple-scattering components from the macrocyclic ligand (Table S4 in the Supporting Information).

Supplementary Material

Refer to Web version on PubMed Central for supplementary material.

Acknowledgments

W.N. at Ewha Womans University acknowledges financial support from the NRF/MEST of Korea through the CRI (2-2012-1794-001-1) and GRL (2010-00353) and from the 2011 KRICT OASIS Project. J.C. at DGIST acknowledges the R&D program of the MEST of Korea (13-BD-0403) for financial support. Portions of this research were carried out at the Stanford Synchrotron Radiation Lightsource, a Directorate of the SLAC National Accelerator Laboratory and an Office of Science User Facility operated for the U.S. Department of Energy, Office of Science by Stanford University. The SSRL Structural Molecular Biology Program is supported by the Department of Energy, Office of Biological and Environmental Research and by the National Institutes of Health, National Institute of General Medical Sciences (including P41M103393), and the National Center for Research Resources (P41RR001209).

References

1. a) Ortiz de Montellano, PR. Cytochrome P450: Structure, Mechanism, and Biochemistry. 3rd ed.. New York: Kluwer Academic/Plenum; 2005. b) Denisov IG, Makris TM, Sligar SG, Schlichting I. Chem. Rev. 2005; 105:2253–2277. [PubMed: 15941214] c) Abu-Omar MM, Loaiza A, Hontzeas N. Chem. Rev. 2005; 105:2227–2252. [PubMed: 15941213] d) Itoh S. Curr. Opin. Chem. Biol. 2006; 10:115–122. [PubMed: 16504568] e) Chufán EE, Puiu SC, Karlin KD. Acc. Chem. Res. 2007;

40:563–572. [PubMed: 17550225] f) Krebs C, Fujimori DG, Walsh CT, Bollinger JM Jr. Acc. Chem. Res. 2007; 40:484–492. [PubMed: 17542550] g) Bruijnincx PCA, van Koten G, Klein Gebbink RJM. Chem. Soc. Rev. 2008; 37:2716–2744. [PubMed: 19020684] h) Green MT. Curr. Opin. Chem. Biol. 2009; 13:84–88. [PubMed: 19345605] i) Ortiz de Montellano PR. Chem. Rev. 2010; 110:932–948. [PubMed: 19769330] j) Shaik S, Cohen S, Wang Y, Chen H, Kumar D, Thiel W. Chem. Rev. 2010; 110:949–1017. [PubMed: 19813749]

2. Nam W. Acc. Chem. Res. 2007; 40:465. and review articles in this special issue; van Eldik R. Coord. Chem. Rev. 2007; 251:1649–1662. Nam W. Acc. Chem. Res. 2007; 40:522–531. [PubMed: 17469792] Cramer CJ, Tolman WB. Acc. Chem. Res. 2007; 40:601–608. [PubMed: 17458929] Himes RA, Karlin KD. Curr. Opin. Chem. Biol. 2009; 13:119–131. [PubMed: 19286415] Gunay A, Theopold KH. Chem. Rev. 2010; 110:1060–1081. [PubMed: 20143877] Yao S, Driess M. Acc. Chem. Res. 2012; 45:276–287. [PubMed: 21875073] Cho J, Sarangi R, Nam W. Acc. Chem. Res. 2012; 45:1321–1330. [PubMed: 22612523] Hohenberger J, Ray K, Meyer K. Nature Commun. 2012; 3:720. [PubMed: 22395611] de Visser J-U, Rohde Y-M, Lee SP, Cho J, Nam W. Coord. Chem. Rev. 2013; 257:381–393. McDonald AR, Que L Jr. Coord. Chem. Rev. 2013; 257:414–428.
3. Kent Barefield E. Coord. Chem. Rev. 2010; 254:1607–1627.
4. Abbreviations used for *n*-TMC: 12-TMC: 1,4,7,10-tetramethyl-1,4,7,10-tetraazacyclododecane; 13-TMC: 1,4,7,10-tetramethyl-1,4,7,10-tetraazacyclotridecane; 14-TMC: 1,4,8,11-tetramethyl-1,4,8,11-tetraazacyclotetradecane; 15-TMC: 1,4,8,12-tetramethyl-1,4,8,12-tetraazacyclopentadecane.
5. a) Cho J, Woo J, Nam W. J. Am. Chem. Soc. 2010; 132:5958–5959. [PubMed: 20392047] b) Cho J, Woo J, Han JE, Kubo M, Ogura T, Nam W. Chem. Sci. 2011; 2:2057–2062.c) Yokoyama A, Han JE, Cho J, Kubo M, Ogura T, Siegler MA, Karlin KD, Nam W. J. Am. Chem. Soc. 2012; 134:15269–15272. [PubMed: 22950528]
6. a) Seo MS, Kim JY, Annaraj J, Kim Y, Lee Y-M, Kim SJ, Kim J, Nam W. Angew. Chem. 2007; 119:381–384. *Angew. Chem. Int. Ed.***2007**, *46*, 377 –380; b) Annaraj J, Cho J, Lee YM, Kim SY, Latifi R, de Visser SP, Nam W. Angew. Chem. 2009; 121:4214–4217. *Angew. Chem. Int. Ed.***2009**, *48*, 4150 –4153.
7. a) Cho J, Jeon S, Wilson SA, Liu LV, Kang EA, Braymer JJ, Lim MH, Hedman B, Hodgson KO, Valentine JS, Solomon EI, Nam W. Nature. 2011; 478:502–505. [PubMed: 22031443] b) Annaraj J, Suh Y, Seo MS, Kim SO, Nam W. Chem. Commun. 2005:4529–4531.
8. a) Jo Y, Annaraj J, Seo MS, Lee Y-M, Kim SY, Cho J, Nam W. J. Inorg. Biochem. 2008; 102:2155–2159. [PubMed: 18842302] b) Cho J, Sarangi R, Kang HY, Lee JY, Kubo M, Ogura T, Solomon EI, Nam W. J. Am. Chem. Soc. 2010; 132:16977–16986. [PubMed: 21062059] c) Sarangi R, Cho J, Nam W, Solomon EI. Inorg. Chem. 2011; 50:614–620. [PubMed: 21142119]
9. a) Kieber-Emmons MT, Annaraj J, Seo MS, Van Heuvelen KM, Tosha T, Kitagawa T, Brunold TC, Nam W, Riordan CG. J. Am. Chem. Soc. 2006; 128:14230–14231. [PubMed: 17076476] b) Cho J, Sarangi R, Annaraj J, Kim SY, Kubo M, Ogura T, Solomon EI, Nam W. Nat. Chem. 2009; 1:568–572. [PubMed: 20711413]
10. a) Rohde J-U, In J-H, Lim MH, Brennessel WW, Bukowski MR, Stubna A, Münck E, Nam W, Que L Jr. Science. 2003; 299:1037–1039. [PubMed: 12586936] b) Fukuzumi S, Morimoto Y, Kotani H, Naumov P, Lee Y-M, Nam W. Nat. Chem. 2010; 2:756–759. [PubMed: 20729896]
11. Some examples of cobalt complexes with peroxo and hydroperoxo ligands: Busch DH, Alcock NW. Chem. Rev. 1994; 94:585–623. Hikichi S, Akita M, Moro-oka Y. Coord. Chem. Rev. 2000; 198:61–87. Hu X, Castro-Rodriguez I, Meyer K. J. Am. Chem. Soc. 2004; 126:13464–13473. [PubMed: 15479103] Hikichi S, Komatsuzaki H, Akita M, Moro-oka Y. J. Am. Chem. Soc. 1998; 120:4699–4710.
12. a) Evans DF. J. Chem. Soc. 1959:2003–2005.b) Loliger J, Scheffold R. J. Chem. Educ. 1972; 49:646–647.c) Evans DF, Jakubovic DA. J. Chem. Soc. Dalton Trans. 1988:2927–2933.
13. a) Jensen KB, McKenzie CJ, Nielsen LP, Pedersen JZ, Svendsen HM. Chem. Commun. 1999:1313–1314.b) Ho RYN, Roelfes G, Hermant R, Hage R, Feringa BL, Que L Jr. Chem. Commun. 1999:2161–2162.c) Nebe T, Beitat A, Würtele C, Dücker-Benfer C, van Eldik R, McKenzie CJ, Schindler S. Dalton Trans. 2010; 39:7768–7773. [PubMed: 20648392]

14. A cobalt – oxo complex was reported recently: Pfaff FF, Kundu S, Risch M, Pandian S, Heims F, Pryjomska-Ray I, Haack P, Met-zinger R, Bill E, Dau H, Comba P, Ray K. Angew. Chem. 2011; 123:1749–1753. *Angew. Chem. Int. Ed.***2011**, *50*, 1711–1715.
15. The involvement of metal–hydroperoxo complexes in oxidation reactions has been the topic of much interest: Franke A, Fertinger C, van Eldik R. Chem. Eur. J. 2012; 18:6935–6949. [PubMed: 22532376] Song YJ, Hyun MY, Lee JH, Lee HG, Kim JH, Jang SP, Noh JY, Kim Y, Kim S-J, Lee SJ, Kim C. Chem. Eur. J. 2012; 18:6094–6101. [PubMed: 22461419] Song YJ, Lee SH, Park HM, Kim SH, Goo HG, Eom GH, Lee JH, Lah MS, Kim Y, Kim S-J, Lee JE, Lee H-I, Kim C. Chem. Eur. J. 2011; 17:7336–7344. [PubMed: 21567491] Fertinger C, Hessenauer-Ilicheva N, Franke A, van Eldik R. Chem. Eur. J. 2009; 15:13435–13440. [PubMed: 19876973] Seo MS, Kamachi T, Kouno T, Murata K, Park MJ, Yoshizawa K, Nam W. Angew. Chem. 2007; 119:2341–2344. *Angew. Chem. Int. Ed.***2007**, *46*, 2291 – 2294; Park MJ, Lee J, Suh Y, Kim J, Nam W. J. Am. Chem. Soc. 2006; 128:2630–2634. [PubMed: 16492048] Ogliaro F, de Visser SP, Cohen S, Sharma PK, Shaik S. J. Am. Chem. Soc. 2002; 124:2806–2817. [PubMed: 11890833] Shaik S, de Visser SP, Ogliaro F, Schwarz H, Schröder D. Curr. Opin. Chem. Biol. 2002; 6:556–567. [PubMed: 12413538] Newcomb M, Shen R, Choi S-Y, Toy PH, Hollenberg PF, Vaz ADN, Coon MJ. J. Am. Chem. Soc. 2000; 122:2677–2686. Liu LV, Hong S, Cho J, Nam W, Solomon EI. J. Am. Chem. Soc. 2013; 135:3286–3299. [PubMed: 23368958] Kim YM, Cho K-B, Wang B, Li C, Shaik S, Na W. J. Am. Chem. Soc. 2013; 135:8838–8841. [PubMed: 23721290]
16. a) Watanabe Y, Nakajima H, Ueno T. Acc. Chem. Res. 2007; 40:554–562. [PubMed: 17567089] b) Groves JT, Watanab Y. J. Am. Chem. Soc. 1988; 110:8443–8452.
17. Armarego, WLF.; Cha, CLL. Purification of Laboratory Chemicals. 6th ed.. Pergamon, Oxford: 2009.
18. Saltzman, H.; Sharefki, JG. Organic Syntheses, Collect. Vol. Vol. V. Wiley: New York; 1973. p. 658
19. Barefield EK, Wargne F. Inorg. Chem. 1973; 12:2435–2439.
20. Sheldick, GM. SHELXTL/PC, Version 6.12 for Windows XP. Madison, WI, USA: Bruker AXS Inc.; 2001.
21. Tenderholt A. Pyspline and QMForge. 2007
22. Mustre de Leon J, Rehr JJ, Zabinsky SI, Albers RC. Phys. Rev. B: Condens. Matter. 1991; 44:4146–4156. [PubMed: 10000060]
23. Rehr JJ, Albers RC. Rev. Mod. Phys. 2000; 72:621–624.
24. Rehr JJ, Mustre de Leon J, Zabinsky SI, Albers RC. J. Am. Chem. Soc. 1991; 113:5135–5140.
25. Avogadro: an open-source molecular builder and visualization tool, Version 1.XX, http://avogadro.openmolecules.net/.
26. George GN. EXAFSPAK and EDG – FIT. 2000

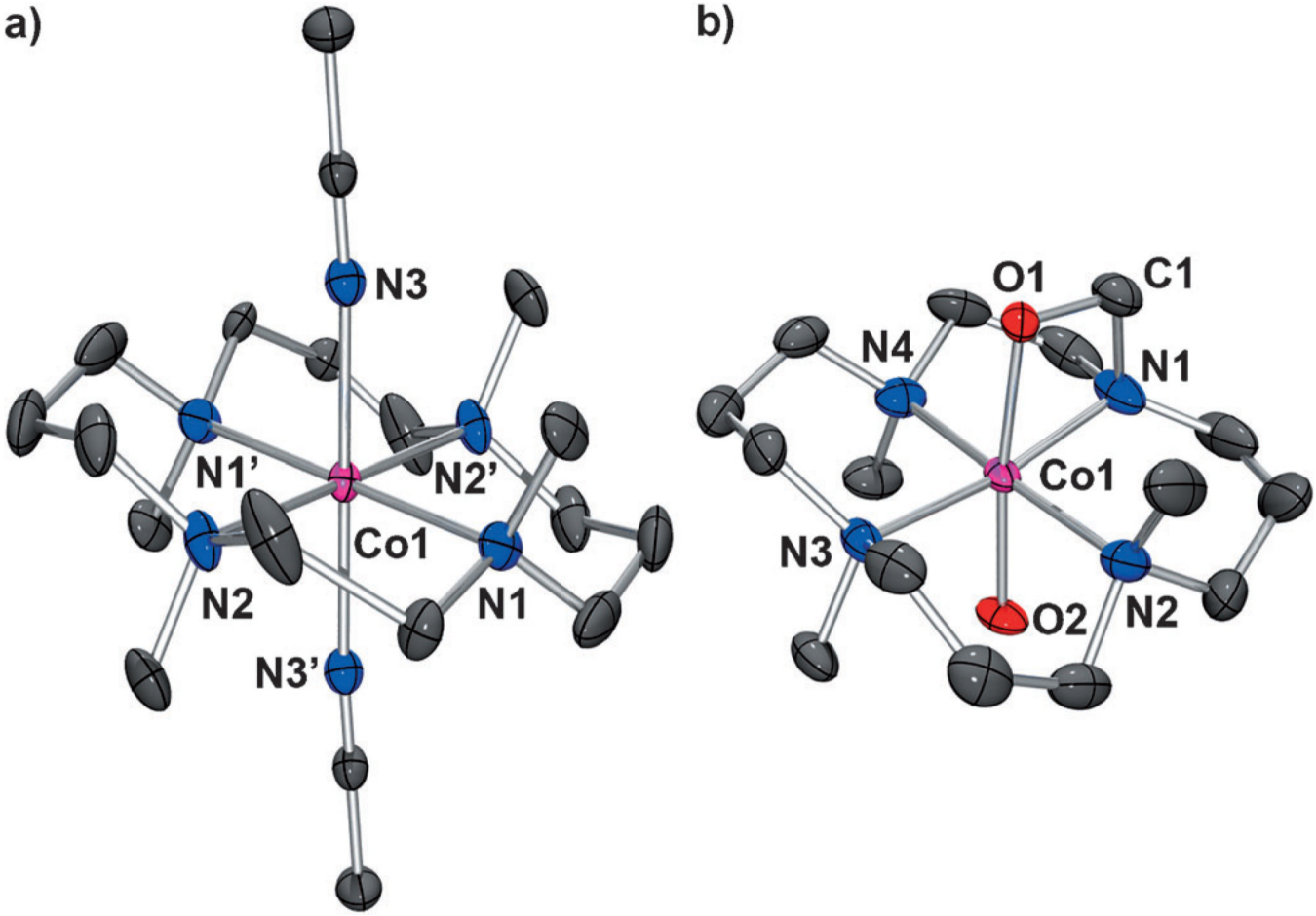

Figure 1.

X-ray crystal structures of a) $[Co^{II}(15\text{-TMC})(CH_3CN)_2]^{2+}$ [**1**•-$(CH_3CN)_2$] and b) $[Co^{III}(15\text{-TMC-}CH_2\text{-O})(OH)]^{+}$ [**4**•(OH)] with thermal ellipsoids drawn at the 30% probability. Hydrogen atoms are omitted for clarity. Selected bond lengths [Å] and angles [°] for [**4**•(OH)]: Co–O1 1.896(3), Co–O2 1.878(4), Co–N1 1.988(5), Co–N2 2.125(5), Co–N3 2.089(4), Co–N4 2.082(5); O1–Co–O2 173.36(17), Co–O1–C1 92.7(3), O1–C1–N1 104.9(4).

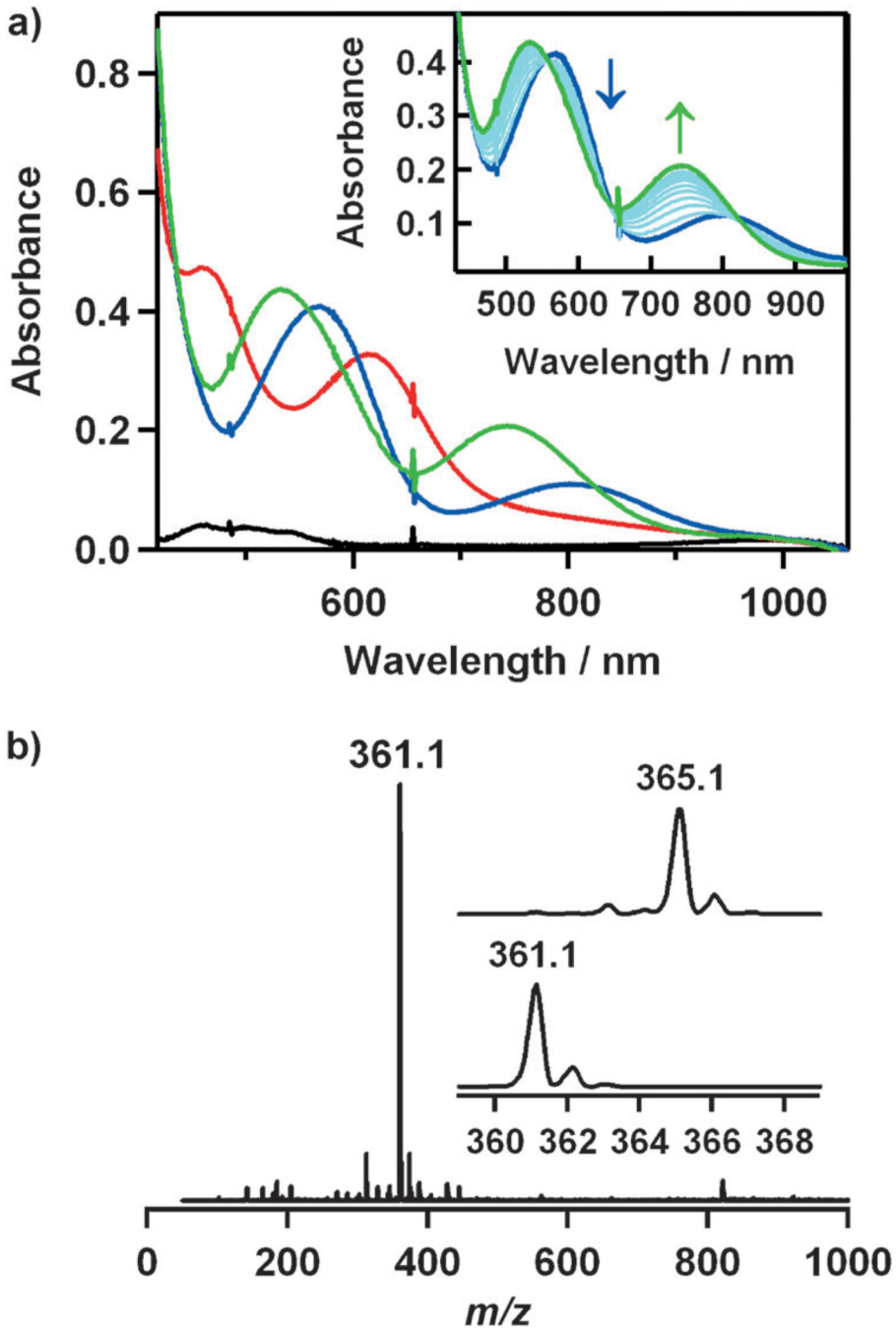

Figure 2.

a) UV/Vis spectra of **1** (black), **2** (red), **3** (blue), and **4** (green). Inset: the conversion of **3** (blue) into **4** (green) in CH_3CN at 0 8C. b) ESI mass spectrum of **2**. Insets: the observed isotope distribution patterns for $[Co(15\text{-}TMC)(O_2)]^+$ at *m*/*z* 361.1 (bottom panel) and $[Co(15\text{-}TMC)\text{-}(^{18}O_2)]^+$ at *m*/*z* 365.1 (top panel).

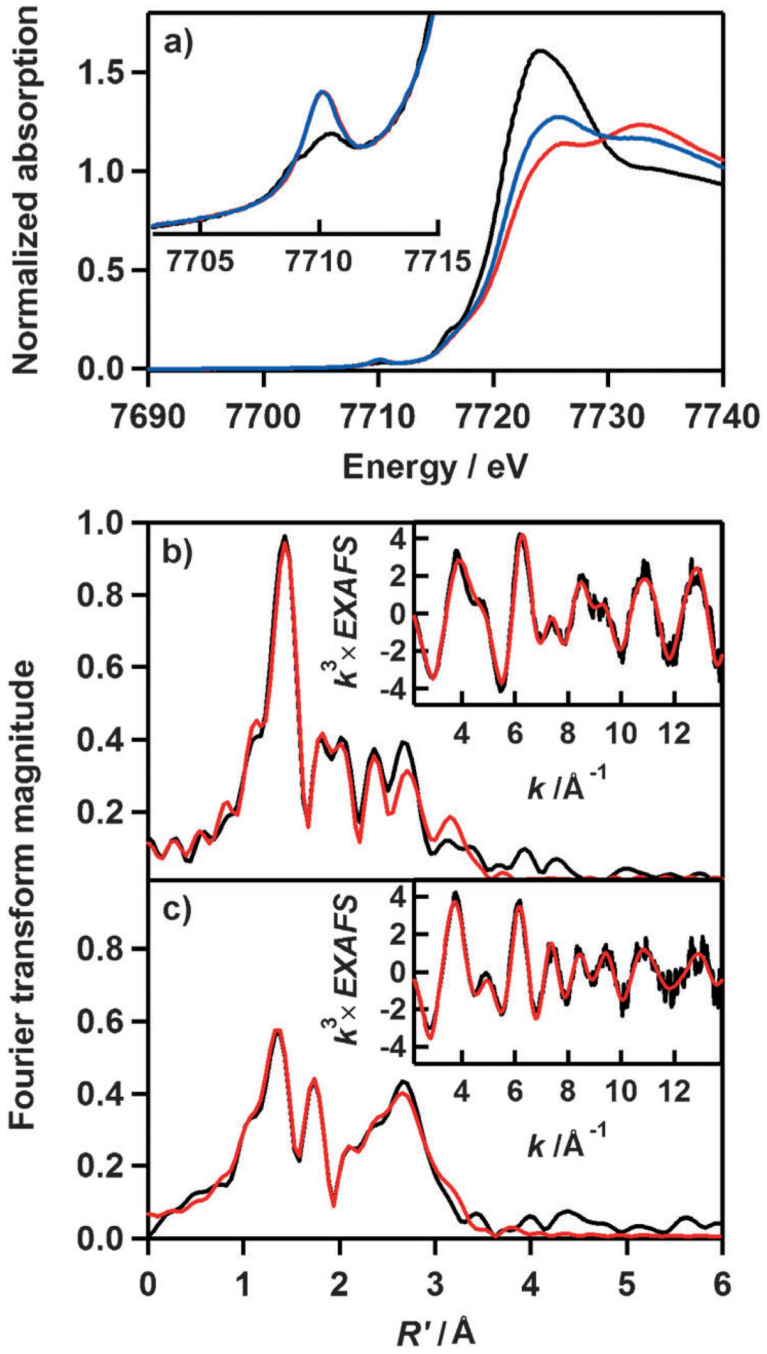

Figure 3.

a) Normalized Co K-edge XAS spectra of **1** (black), **2** (red), and **3** (blue). The inset shows the pre-edge region. FEFF fits (black) to the non-phase-shift-corrected Fourier transforms (red) and the corresponding EXAFS data (insets, red) for b) **2** and c) **3**.

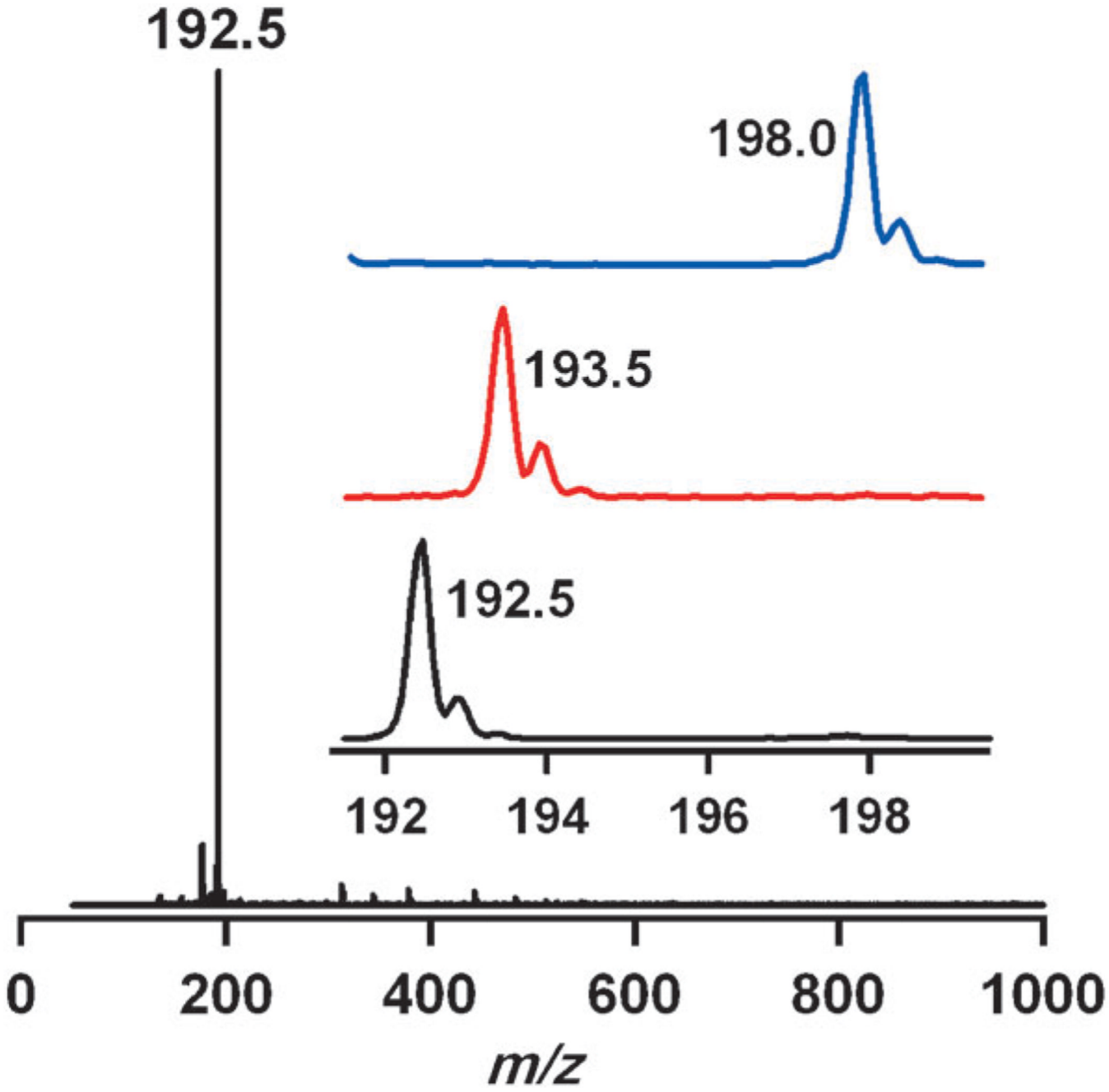

Figure 4.
ESI mass spectrum of **4**. The insets show the observed isotope distribution patterns for **4**-^{16}O, **4**-^{18}O, and **4**-CD_3.

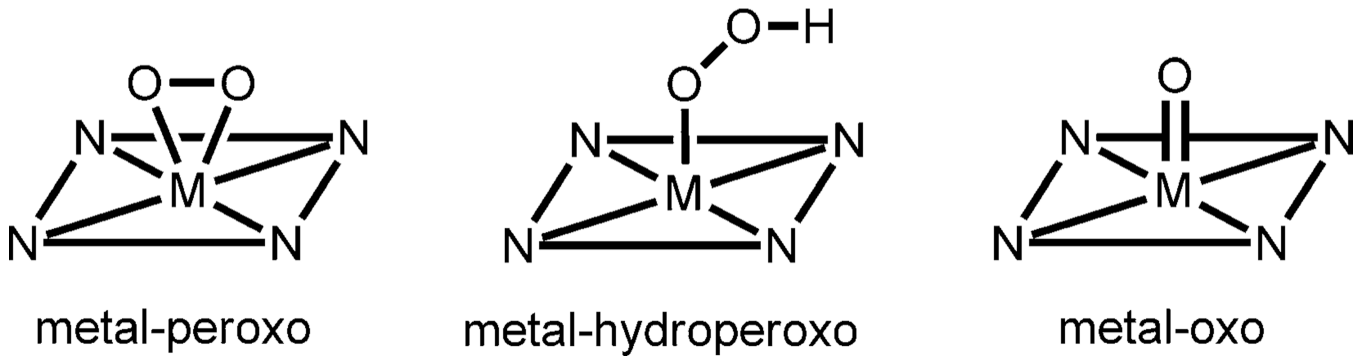

scheme 1.
A schematic drawing of metal–peroxo, metal–hydroperoxo, and metal–oxo complexes.

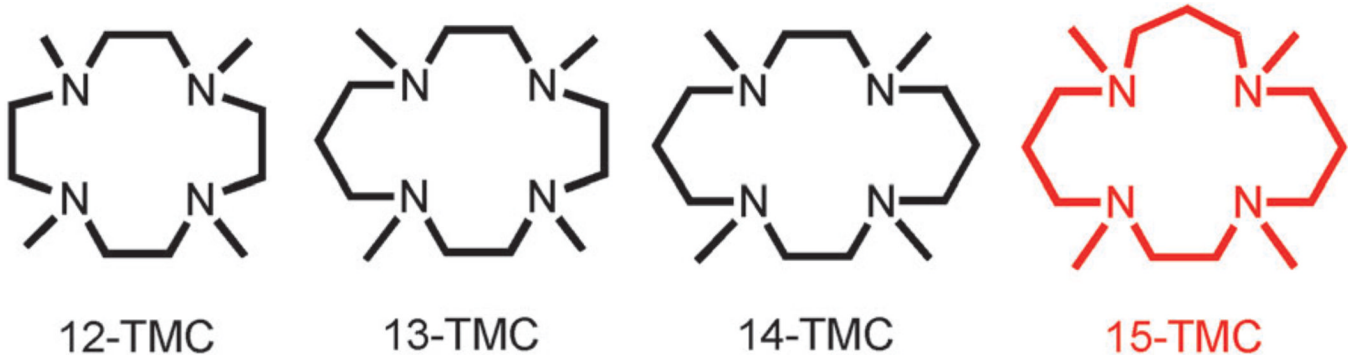

scheme 2.
A schematic drawing of *n*-TMC ligands.[4]

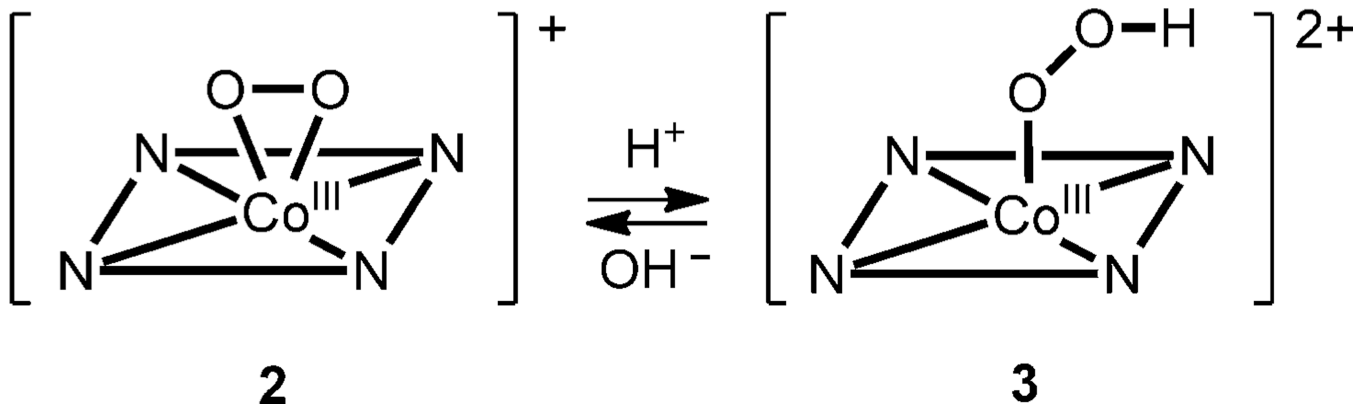

2 **3**

scheme 3.

A reversible acid–base equilibrium between the cobalt(III)–peroxo (**2**) and cobalt(III)–hydroperoxo (**3**) complexes.

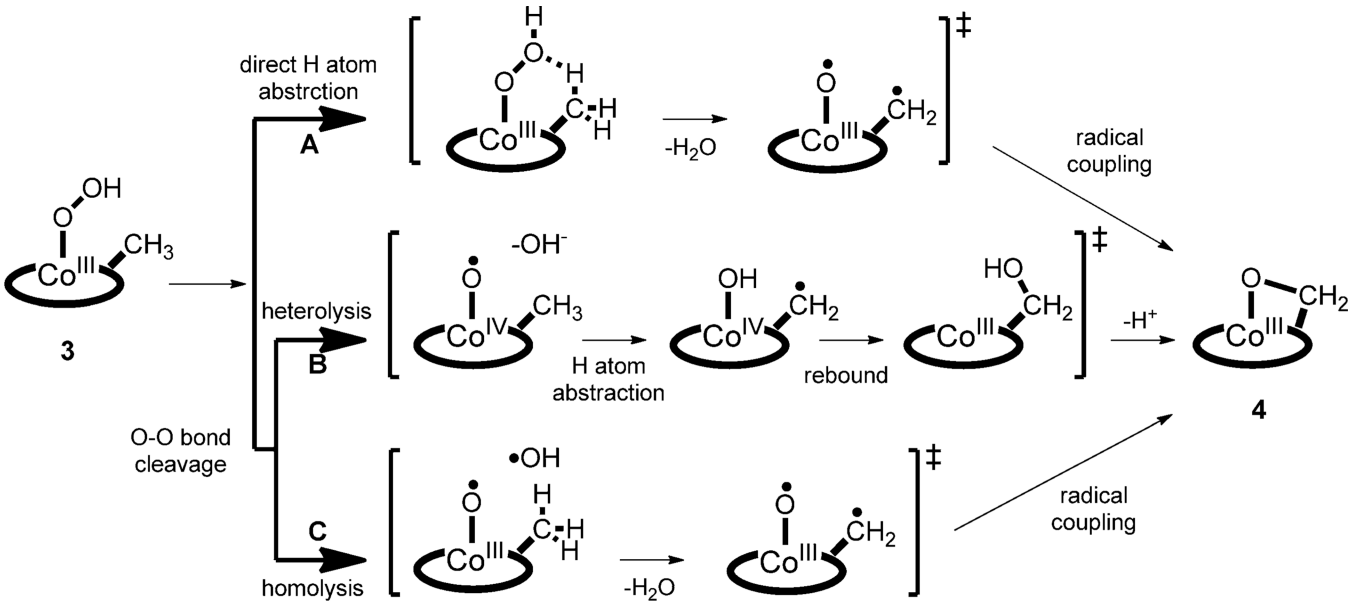

scheme 4.

Possible mechanisms for the conversion of **3** to **4**